PCCP

Photoreductive Dissolution of Cerium Oxide Nanoparticles and Their Size-Dependent Absorption Properties

Journal:	*Physical Chemistry Chemical Physics*
Manuscript ID	CP-ART-12-2019-006579.R1
Article Type:	Paper
Date Submitted by the Author:	28-Jan-2020
Complete List of Authors:	Pettinger, Natasha; Montana State University, Department of Chemistry and Biochemistry Empey, Jennifer; Ohio State University, Chemistry and Biochemistry Fröbel, Sascha; Heinrich Heine Universität Düsseldorf, Institut für Physikalische Chemie Kohler, Bern; Ohio State University, Chemistry and Biochemistry

SCHOLARONE™
Manuscripts

Photoreductive Dissolution of Cerium Oxide Nanoparticles and Their Size-Dependent Absorption Properties

Natasha W. Pettinger, Jennifer M. Empey, Sascha Froebel,† and Bern Kohler*

Department of Chemistry and Biochemistry, The Ohio State University, 100 West 18th Avenue, Columbus, Ohio 43210, United States

† Permanent address: Covestro Deutschland AG, Kaiser-Wilhelm-Allee 60, 51373 Leverkusen, Germany

*Corresponding Author: Bern Kohler, kohler.40@osu.edu, Tel: +1 614-688-2635

Abstract

Cerium oxide has attracted attention recently for its photocatalytic properties, but there are gaps in understanding its performance, especially at low and high pH. UV irradiation of ceria nanoparticles causes electrons from photogenerated electron-hole pairs to localize as small polarons, yielding Ce^{3+} ions. In pH 10 solution, ceria nanoparticles capped with polyacrylic acid ligands can accumulate large numbers of Ce^{3+} defects as revealed by strong bleaching of the absorption onset. In contrast, we show that UV irradiation of several-nanometer diameter ceria nanoparticles in acidic (pH < 3) aqueous solution releases Ce^{3+} ions into solution with a quantum yield that approaches 70% and that varies with excitation wavelength, particle size, and the presence of a hole scavenger (glycerol) on the nanoparticle surface. The instability of Ce^{3+} at the nanoparticle surface and the ability of electron small polarons to migrate to the surface by hopping strongly suggest that nanoceria is fully oxidized and essentially free of Ce^{3+} centers at pH < 3. Efficient photoreduction and the excellent stability of unirradiated nanoparticles make it easy to shrink the nanoparticles using only light, while maintaining them in a fully oxidized state. This enables study of the size-dependent absorption properties of ceria nanoparticles that are free of Ce^{3+} defects. No evidence of quantum confinement is observed, consistent with highly localized excited states. The observed quantum yields of photoreduction are higher than reported for other metal oxides, revealing that a significant fraction of electron-hole pairs are available for driving surface redox reactions, even in fully oxidized particles.

INTRODUCTION

CeO_2, or ceria, is a reducible oxide prized for its excellent catalytic activity.[1] One of the most interesting characteristics of ceria is its redox mutability or ability to stabilize or accommodate Ce^{3+} ions in its fluorite lattice. In high-temperature reducing conditions, ceria is transformed into nonstoichiometric ceria, CeO_{2-x}, in which the loss of a lattice oxygen atom is compensated by the reduction of two Ce^{4+} ions to Ce^{3+} ions. The resulting oxygen vacancies promote oxide ion mobility, allowing ceria to act as an oxygen buffer in automobile catalytic converters and as an electrolyte in solid oxide fuel cells.[2] Oxygen vacancies themselves also play a very important role in catalysis.[3]

There is growing interest in the use of ceria nanoparticles ("nanoceria") in room-temperature aqueous solution for photocatalysis.[2, 4-9] Considerable confusion persists, however, about exactly how Ce^{3+} centers influence photocatalytic events.[4, 6, 7, 10] CeO_2 and TiO_2 have similar absorption onsets in the near UV, but differences in their photocatalytic performance are poorly understood. Nanoceria has also been of great interest for medical therapeutics due to its ability to store and deliver redox equivalents in a manner that mimics natural enzymes.[11-17] This ability is believed to result from the Ce^{3+} content.[18]

Given the importance of Ce^{3+} defects to the catalytic properties of nanoceria, much effort has been devoted to understanding the amount of Ce^{3+} in ceria nanoparticles of various sizes.[19-23] In general, smaller nanoparticles are believed to have a higher fraction of Ce^{3+} ions than larger particles. Thus, Deshpande et al.[21] studied nanoceria by x-ray photoelectron spectroscopy (XPS) and estimated that 44% and 29% of cerium ions are in the +3 oxidation state in 3 nm and 6 nm CeO_2 particles, respectively. Lee et al. [22] reported a Ce^{3+} content of 45% in their 3.5 nm diameter nanocrystals. However, the XPS technique can overestimate the Ce^{3+} concentration due to

reduction of Ce^{4+} by the X-ray flux.[24] More work is needed, especially because high-vacuum conditions favor the formation of CeO_{2-x}, leading to oxygen vacancies, which may not be present in aqueous solution.[23]

A further debate concerns the possibility of observing quantum confinement effects in CeO_2. Quantum confinement causes an increase in the band gap energy of many inorganic nanoparticles or quantum dots as their size decreases below the size of the exciton produced by photoexcitation.[25-27] Some researchers attribute the blue shift seen in the absorption onset of ceria nanoparticles of decreasing size to a quantum confinement effect.[28-30] Still others report no change with size[31], or even a decrease in the band gap with decreasing size for ceria nanoparticles < 10 nm.[7, 32-34] This debate is coupled to the one about Ce^{3+} content, because as pointed out by Tsunekawa et al.,[35, 36] blue shifts in absorption may instead be due to size-dependent concentrations of Ce^{3+} defects in nanoceria.

Motivated by two recent studies showing that UV irradiation increases the Ce^{3+} content of nanoceria,[37, 38] we began a study of the size-dependent absorption properties of ceria nanoparticles. In the course of our investigation, we discovered that UV irradiation of nanoceria in highly acidic solution results in photoreductive dissolution. Photoreductive dissolution has been observed in a number of metal oxides,[39-45] but this phenomenon has not been described previously in cerium oxide to the best of our knowledge. It is notable for its high quantum yield, even in the absence of a sacrificial reductant, and for the virtually negligible rate of thermal dissolution in the absence of light. We use the ability to continuously change the size of ceria nanoparticles with UV light to gain insights into the size-dependent absorption properties of this important, redox-active nanomaterial. We also present initial observations showing that Ce^{3+}

ejection from ceria nanoparticles to the solution phase is highly sensitive to excitation wavelength and the presence of an adsorbed hole scavenger.

METHODS

Two types of ceria nanoparticles were studied, which differ in size and in their passivating ligands. One sample of ceria nanoparticles (hereafter, ceria-CAN) was synthesized as described in ref. 46. Briefly, ~160 mg of cerium(IV) ammonium nitrate (CAN), $(NH_4)_2Ce(NO_3)_6$, (99% purity, Acros Organics) was dissolved in 40 mL of purified water from a water ultrapurifier (Millipore Synergy) and allowed to age for a minimum of 1 day, yielding a stock dispersion with approximately 1.3 mg mL^{-1} nanoceria, assuming complete conversion of CAN to CeO_2. Ceria-CAN nanoparticles form spontaneously at low pH at room temperature when CAN is dissolved in mM concentrations in water.[46] The ceria-CAN nanoparticles were studied following dilution of the stock dispersion, but were never isolated after synthesis because evaporation of the solvent can transiently decrease the pH enough to revert some of the nanoceria to the starting cerium(IV) salt. Also, precipitating ceria-CAN nanoparticles with base causes the particles to agglomerate irreversibly.

The second nanoceria sample (hereafter, ceria-AA) was purchased from a supplier (Alfa Aesar, stock no. 40125) as a pH 3.0 colloidal dispersion (20% by mass) in water containing 0.4 M acetate ions and proprietary passivating ligands. The as-received dispersion was diluted 100-fold with aqueous 0.01 M $HClO_4$ (Fluka Analytical) to create a stock dispersion with an approximate nanoceria concentration of 2.4 mg mL^{-1}. Experiments were performed on samples prepared by diluting the ceria-CAN and ceria-AA stock dispersions with aqueous 0.01 M $HClO_4$ to yield samples with absorbance values at 289 nm between 1 and 3 in a 1 cm path length.

Dilution was performed with aqueous perchloric acid to provide buffering against a pH increase resulting from the consumption of protons during photodissolution (see below). Perchloric acid absorbs negligibly above 250 nm and perchlorate is a non-complexing anion. The resulting solutions had pH values between 1.9 and 2.0, and the pH did not change during UV irradiation within experimental uncertainty.

Photodissolution quantum yields were determined by irradiating solutions with the 75 W xenon arc lamp in a commercial fluorometer (QuantaMaster 8075-22, Horiba) and measuring the change in the solution absorbance at 289 nm produced by the absorbed photon flux. Irradiation was carried out at 265 nm and 300 nm in 1 cm path length cuvettes on nanoceria dispersions with an initial absorbance of ~3 at 290 nm. The entrance and exit slits in the excitation spectrometer between the lamp and the sample were set to the maximum band pass of 8 nm. Additional details are in section 1 of the Supporting Information (SI).

All UV irradiation experiments to study photodissolution were performed on aqueous dispersions of ceria nanoparticles in 1 cm path length cuvettes made of fused silica in a Rayonet carousel photoreactor (Southern New England Ultraviolet Co.) equipped with mercury arc lamps. The samples had an initial absorbance of ~1 at 289 nm and were continuously stirred during irradiation using a micro stir bar and were capped to prevent solvent evaporation. Stirring was essential for obtaining reproducible absorbance changes upon irradiation.

RESULTS AND DISCUSSION

Nanoceria characterization. The ceria nanoparticles were characterized by X-ray diffraction (XRD) and transmission electron microscopy (TEM) as described in section 2 of the SI. Scherrer

analysis of peak broadening in the measured XRD spectra (Figure S1) yielded average crystallite diameters of 6.8 ± 0.8 nm and 3.1 ± 0.3 nm for the ceria-AA and ceria-CAN nanoparticles, respectively (Table S1). Manual sizing of particles in TEM images gave average diameters of 5.7 nm and 4.3 nm for the ceria-AA and ceria-CAN particles, respectively, and revealed that the nanoparticles are heterogeneous in size and shape.

TEM images show that the ceria-AA particles have diameters ranging between 1 and 12 nm (Figure S2a), while the ceria-CAN particles are slightly smaller with diameters of between 1 and 9 nm (Figure S2b). Larger agglomerates are seen in both samples (Figure S2). The agglomerates are thought to be an artifact of the TEM sample preparation as neither sample exhibits the light scattering that would be expected in the UV-vis absorption spectra (see Figure 1), if structures on the order of 100 nm or larger were present. HR-TEM images reveal that the ceria-CAN particles are polycrystalline (Figure S3), while the loose agglomerates that predominate in the ceria-AA nanoparticles make it difficult to confirm whether they consist of single crystals or not (Figure S4).

The UV-vis absorption spectra of both nanoceria samples in water (Figure 1) are similar with an onset near 3 eV (400 nm). Absorption coefficients per mole of cerium ions (left axis) and per unit mass concentration (right axis) are graphed in Figure 1 vs. photon energy (and wavelength) for both nanoceria samples. These values were determined as described in section 1 in the SI. The subtle differences in the spectra of the two samples are reproducible and will be discussed later.

Photoreductive Dissolution in Acidic Solution. Both nanoparticle suspensions experience a striking loss of absorption when irradiated with a mercury lamp at pH 1.9. Identical results are obtained with air-free (Ar-purged) and air-saturated samples. Results for ceria-AA are shown in

Figure 2, but similar results are obtained with ceria-CAN nanoparticles (Figure S5). Photoinduced bleaching is also observed in both samples at additional pH values below 3. No change in absorption is observed in acidic aqueous solution in the absence of irradiation. As reported previously, the absorption spectrum of ceria-CAN in an as-synthesized dispersion at pH 2 is unchanged after storage in the dark for one year.[46]

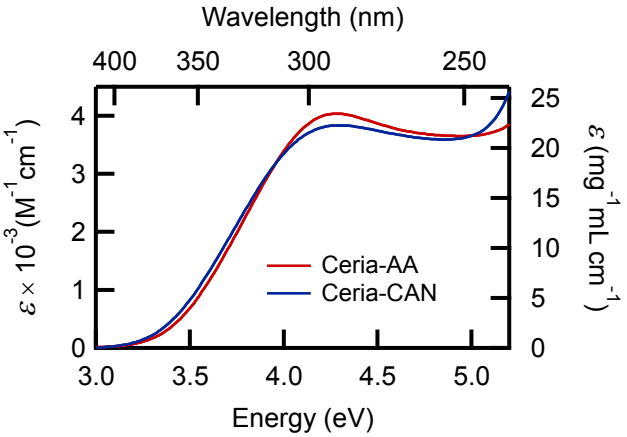

Figure 1. Steady-state UV-vis absorption spectra of ceria-AA (red curve) and ceria-CAN (blue curve) measured in water at pH 1.9.

With extended UV irradiation, several peaks are revealed at wavelengths shorter than 260 nm (Figure 2a). The final spectrum after 150 minutes of irradiation has a weak peak at 300 nm (4.13 eV) and a stronger doublet with maxima at 239 nm (5.19 eV) and 252 nm (4.92 eV) (Figure 2b). This spectrum matches the absorption spectrum of the Ce^{3+} aqua ion, Ce^{3+}(aq), which has five bands between 270 nm (4.59 eV) and 200 nm (6.20 eV) and a weaker band at 300 nm (4.13 eV).[47, 48] For reference, this spectrum is shown by the solid black curve in Figure 2b. The distinctive quintet of bands arises from 4f→5d transitions involving the excited $^2D(5d^1)$ multiplet of the cerium 5d electron and is highly diagnostic of Ce^{3+}(aq). The two curves in Figure 2b differ

above 5.3 eV due to absorption by acetate ions and surfactants added to the ceria-AA suspension by the manufacturer. In Figure 2a, each of the colored curves is a linear combination of the absorption spectrum of ceria prior to UV irradiation and the spectrum of Ce^{3+}(aq) (black curve in Figure 2b). The excellent agreement with the measured spectra (open circles) demonstrates that the spectra in Figure 2a are internally linear,[49] meaning that any spectrum in the set can be generated from any two of the others.

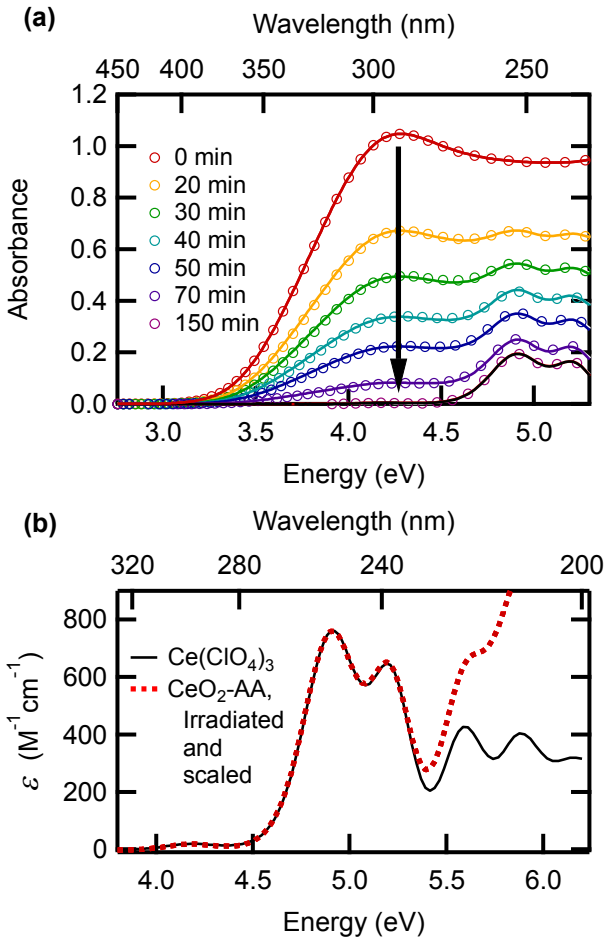

Figure 2. (a) Absorption spectra of ceria-AA nanoparticles in pH 2 aqueous solutions after irradiation with a mercury lamp for the times indicated (open circles). The arrow indicates increasing irradiation time. The solid lines are fit curves computed as described in the text. (b) The absorption spectrum of ceria-AA nanoparticles after 150 minutes of irradiation (red dashed curve) scaled to match the long wavelength peaks in the absorption spectrum of $Ce(ClO_4)_3$ (aq) measured at pH 6 (black solid curve).

In Figure 2a, the absorbance at 290 nm before irradiation is approximately five times greater than the absorbance at 252 nm after the particles have been completely transformed into Ce^{3+}(aq). As described in section 1 of the SI, a value of 4100 ± 200 M^{-1} cm^{-1} is determined for the molar absorption coefficient (per mole of metal ions) of the ceria-AA nanoparticles at 290 nm using the literature value of 750 ± 70 M^{-1} cm^{-1} for Ce^{3+}(aq) at 254 nm.[50] Ceria is an excellent UV absorber with an absorption coefficient larger than that of most metal oxides. To cite one example, a value of 1100 M^{-1} cm^{-1} (per mole of Zn ions) for ZnO nanoparticles at 250 nm can be derived from data in ref. 51.

Photobleaching due to the reduction of cerium(IV) in nanoceria dispersions using UV irradiation was described in two recent reports.[37, 38] Klochkov et al.[38] showed that citrate-stabilized ceria nanoparticles 2 and 9 nm in size can be photoreduced by UV in pH 6.5 – 7.0 aqueous solutions. Damatov et al.[37] demonstrated that Ce^{3+} ions could be accumulated in nanoceria in cyclohexane/THF (2:1) solution and in water under UV irradiation. In the UV irradiated solutions in ref. 37, ethanol was added as a hole scavenger. In both studies, the nanoparticles are reduced by UV excitation, but there is no evidence that Ce^{3+} is leached from the particles. Even when the peak ceria absorbance decreases by more than 50% in response to

irradiation, narrow peaks like the ones seen in Figure 2a near 5.0 eV are not seen in the spectra in ref. 37. The fact that UV-irradiated nanoceria undergoes redox reactions when a species like 1,4-benzoquinone is added after photoreduction[37] is further evidence that Ce^{3+} ions are retained for significant periods of time within the nanoparticles.

To confirm that Ce^{3+} ions are only released from nanoceria by UV irradiation in strongly acidic conditions, ceria-CAN particles were capped with poly(acrylic acid) (PAA) following the procedure of Sehgal et al.[52] and suspended in pH 10 solution. The PAA ligands prevent particle agglomeration and stabilize nanoceria in alkaline solution. The absorption spectra of PAA-capped and uncapped particles in acidic conditions agree well at wavelengths longer than 250 nm. Differences at shorter wavelengths are due to absorption by PAA. Without UV exposure, the PAA-capped ceria-CAN particles, like the non-PAA-capped particles maintained in the dark at lower pH, show no changes in absorption (Figure 3a). Irradiating this solution with the UV radiation from a mercury lamp causes pronounced photobleaching and a progressive blue shift in the absorption maximum (Figure 3b). In addition, the structure seen near 5.0 eV in Figure 2a, which is diagnostic of Ce^{3+}(aq), is not observed, indicating that no cerium ions are lost from the particles. Even after extended UV irradiation, the absorbance measured at the maximum near 290 nm could not be decreased by more than 35% of the starting absorbance (Figure 3b). These findings show that Ce^{3+} defects created by UV irradiation of the PAA-capped nanoceria can be accumulated up to a saturation limit at higher pH similar to the results in refs. [37, 38]. The blue shift of the absorption maximum seen in Figure 3b confirms the effect described by Tsunekawa et al.,[35, 36] and may be due to band filling as excess electrons fill empty states, preventing low energy transitions.[25]

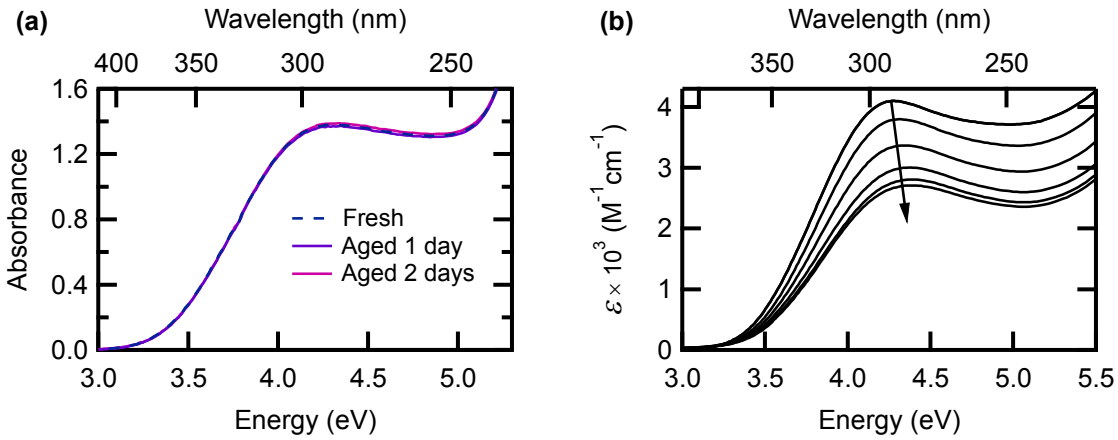

Figure 3. (a) The absorption spectrum of a freshly prepared PAA-capped ceria-CAN solution in pH 10 aqueous solution compared with spectra recorded from the same solution stored in the dark one and two days later, (b) UV-vis spectra recorded after doses of UV irradiation that increase in the direction of the arrow using PAA-capped ceria-AA nanoparticles at pH 10.

Although photoreduced TiO_2[25] and ZnO[53] nanoparticles react rapidly with O_2, photoreduced nanoceria is metastable in air for hours. Nonetheless, photoreduced nanoceria dispersions left standing overnight recover toward their pre-irradiated state, implicating a slow redox reaction, which was not studied further. Klochkov et al.[38] also reported the slow recovery of the bleached absorbance of photoreduced nanoceria. Our observation that Ce^{3+} defects can be stably accumulated in pH 10 solution, but are released to the solvent when pH < 3 indicates that pH plays a critical role in dissolution. This is fully consistent with the cerium Pourbaix diagram determined by Yu et al.,[54] which predicts that aqueous Ce^{3+}(aq) is predominant at pH < 2 and stable against oxidation by O_2, while ceria is favored at pH > 6. Because Ce^{3+} ions are oxidized to Ce^{4+} in alkaline conditions,[54, 55] any Ce^{3+} ions that are ejected should be oxidized and re-deposited on the particles, preventing net dissolution.

Interestingly, the same Pourbaix diagram predicts that the reductive dissolution of cerium oxide is thermodynamically feasible with water as a reducing agent at pH < 4 – 6,

$$CeO_2 + 3H^+ = Ce^{3+} + 3/2\ H_2O + ¼\ O_2 \qquad \Delta G^0 = -42\ kJ\ mol^{-1} \qquad (1)$$

Indeed, Plakhova et al.[56] reported that reductive thermal dissolution does occur in aqueous nanoceria dispersions and that dissolution is more important at low pH as expected from reaction 1. Using ICP-MS to quantify the concentration of Ce^{3+} present in the supernatant isolated from acidic aqueous dispersions of ceria nanoparticles, they determined that the concentration of Ce^{3+} varies at pH ≤ 4.5 as $\log\left[Ce^{3+}\right] = -1.7 - 0.5\text{pH}$. For the pH 2 conditions in our experiments, this relation predicts an equilibrium Ce^{3+} concentration of 2 mM. As this is several times higher than the total cerium concentration in our nanoparticle dispersions, they should dissolve completely, contrary to observations. Such large changes in Ce^{3+} concentrations would also be easy to detect through spectral changes, but our nanoparticles show unchanged absorption spectra even after many months. Further study is needed, but it is possible that differences in the initial Ce^{3+} content of the nanoparticles are important. We believe that our study provides evidence that although thermal reductive dissolution is thermodynamically allowed in acidic conditions, the kinetics are prohibitively slow for fully oxidized nanoceria.

TEM images were recorded of irradiated and nonirradiated aliquots from the same acidic nanoceria dispersion to verify that UV light shrinks the particles. TEM images of ceria-AA nanoparticles with (Figure S6a) and without (Figure S6b) a UV dose sufficient to decrease the absorbance at 289 nm by 90% were analyzed by manually sizing the nearly 200 nanoparticles seen in each image. The resulting size distributions (Figure S7) show that UV irradiation decreased the average particle size from 5.7 nm to 3.6 nm. For ceria-CAN nanoparticles in water, irradiation sufficient to decrease the absorbance at 289 nm by 67% caused the mean crystallite

diameter within the polycrystalline particles to shrink from 3.1 nm to 2.0 nm (Figures S8 and S9).

The absence of quantum confinement effects (see below) suggests that the absorption cross section is proportional to the number of formula units of CeO_2, or, equivalently, the nanoparticle volume. This behavior is seen for many inorganic nanoparticles provided that excitation is far enough above the band gap.[26, 27, 51] Under these conditions, the loss of absorbance is proportional to the total volume change experienced by all particles. However, without additional information about the precise morphologies of the ceria-CAN and ceria-AA nanoparticles, it is difficult to precisely correlate size and absorbance changes.

Photodissolution of ceria has not been reported previously to the best of our knowledge, but nanoceria does undergo thermal dissolution in acidic solutions containing molecular reductants.[16, 57, 58] Ni et al.[16] reported that the addition of H_2O_2 to nanoceria at pH 2.58 increased the amount of Ce^{3+} in solution. These authors proposed that adding an easily oxidized substance or a good ·OH scavenger promotes reductive dissolution at low pH.[16] Peng et al.[57] reported that polycrystalline ceria nanoparticles (3 – 6 nm diameter) gradually dissolve in pH 4.0 citrate buffer solution when oxidizable dye molecules are present. Schwabe et al.[58] reported that the dissolution of nanoceria in phosphate-free plant growth solution is enhanced when the pH is less than 4.5. In these studies, thermal electron transfer with an adsorbate forms a Ce^{3+} center near the surface of a cerium oxide nanoparticle that then desorbs into the solution. Our results show that a sacrificial reductant or hole scavenger is not needed either to observe photodissolution (Figure 2a) or photoreduction (Figure 3b). However, we will demonstrate below that the presence of a hole scavenger further enhances the quantum yield of photoreduction.

Excess electron localization in nanoceria. Excess electrons in CeO_2, whether they are introduced by photoexcitation, chemical doping, or oxygen vacancies, form small polarons in which the electron is localized in a 4f orbital on a single Ce ion, reducing a Ce^{4+} site to Ce^{3+}.[59] Estimates of the activation barrier height for polaron hopping in ceria range between 0.1 and 0.4 eV, according to experiment[60] and calculations.[59, 61, 62] These values are low enough to allow a polaron at room temperature to move by hopping until a deep trap is encountered. Because the polaron is stabilized to a greater extent at the surface than in the bulk, electron small polarons (i.e., Ce^{3+} defects) are expected to move to and be concentrated at the surface, consistent with previous reports.[19, 20, 24, 58] Based on these considerations, we expect that virtually all Ce^{3+} centers in photoreduced ceria nanoparticles like the ones in Figure 3b are present at the surface. Perhaps the most direct evidence that Ce^{3+} defects are localized at the surface comes from imaging experiments on ceria nanoparticles dispersed in ethanol and then dried on a holey carbon grid, showing that up to 50% of cerium ions in a 0.8 nm thick layer near the surface are reduced, depending on the surface facet investigated.[63]

Strong support for the conclusion that Ce^{3+} ions accumulate predominantly at the surface of a ceria nanoparticle also comes from the observation by Klochkov et al.[38] that a greater percentage of the initial absorbance could be bleached in smaller 2 nm than in larger 9 nm diameter particles. A greater fraction of all Ce ions are at the surface of smaller particles, allowing higher Ce^{3+}/Ce^{4+} ratios to be achieved by UV irradiation. The maximum decrease in absorbance of 35% seen with the PAA-capped ceria-AA nanoparticles (Figure 3b) should be compared with the rough estimate that 17 - 24% of all cerium ions are present at the surface of a 6.8 nm-diameter nanoparticle (Table S2). This suggests that essentially every Ce ion at the surface and many subsurface ions are reduced, possibly due to the formation of a shell structure of Ce_2O_3. It has

recently been shown by Ghoshal et al.[64] that nanodots of Ce_2O_3 are unexpectedly stable at ambient conditions.

The observation of hydrated Ce^{3+} ions in the aqueous phase upon UV irradiation indicates that Ce^{3+} is unstable on the surface of nanoceria in highly acidic aqueous solutions. Given that excess electrons (Ce^{3+} ions) in the nanoparticle interior most likely recombine with holes or hop to lower surface traps strongly suggests that ceria nanoparticles in highly acidic aqueous solution are fully oxidized and free of Ce^{3+} defects. Paun et al.[23] noted that nanoceria produced by the hydrolysis of a Ce(IV) precursor salt is unlikely to contain significant amounts of Ce^{3+}, but exposure to intense X-rays can increase the amount of Ce^{3+} in a manner that depends on nanoparticle size. UV radiation readily forms Ce^{3+} sites in nanoceria that are released into solution in low pH conditions, but accumulate when the pH is higher as shown here and in refs. [37, 38].

Because nanoceria still absorbs very weakly at 400 nm, we sought to determine whether room lights photoreduce aqueous nanoceria samples. Irradiating a freshly prepared ceria-AA sample (pH 2) for several hours at 400 nm using the excitation lamp in the fluorometer produced no significant change in absorbance. Based on this result, we suggest that neither photodissolution nor photodoping occur at significant rates in nanoceria samples exposed to visible lighting.

No evidence of quantum confinement in nanoceria. The ability to shrink ceria nanoparticles with light while maintaining their Ce^{3+} content near zero makes it possible to disentangle size effects from those arising from Ce^{3+} content. Although light can be used to shrink the nanoparticles "to nothing", the smallest nanoparticles that can be characterized spectrally will be

limited by the minimum sensitivity of the absorbance measurements. By making the crude approximation that the nanoparticles are spherical and remain so during dissolution, the number of Ce ions remaining in a nanoparticle is proportional to the cube of the diameter. At a wavelength like 320 nm where there is negligible absorption by Ce^{3+}(aq) (Figure 2b), the decrease in absorbance is due solely to the loss of Ce^{4+} ions. If we conservatively assume that we can no longer observe subtle spectral changes when the spectra have decreased to 1% of their initial absorbance, then the smallest nanoparticles that can be characterized are ones that experience a mass loss of 99%, corresponding to a decrease in diameter by a factor of $(0.01)^{-1/3}$ or 4.6. After 99% mass (or absorbance) loss, the average ceria-AA nanoparticle will be 1.5 nm in diameter, corresponding to a cluster of ~40 Ce ions.

For the smaller ceria-CAN nanoparticles, 99% absorbance loss corresponds to a final particle diameter of ~1 nm, but the polycrystallinity of the ceria-CAN particles may result in a final particle that is more amorphous. In other words, the ceria-CAN particles likely retain their polycrystallinity as they shrink and the smallest quantifiable particle diameter may contain large numbers of Ce^{3+} ions in grain boundary vs. crystalline sites. The results in Figure 2a showing that the measured absorption spectra can be fit to just two basis spectra throughout dissolution suggest that the absorption spectrum of crystalline cerium oxide is unchanged down to the smallest particle size that can be detected in our measurements (~1.5 nm for ceria-AA).

Finite difference spectra calculated from the spectra in Figure 2a provide a more sensitive means to assess subtle changes as the ceria nanoparticles dissolve and attain very small sizes. We subtracted the spectrum recorded after irradiating the sample for a time t_2 from one recorded after irradiating for a time t_1 with $t_2 > t_1$ and then multiplied the resulting curve by a positive constant to make its minimum value equal −1. The normalized difference spectra calculated in

this way are shown in Figure 4 for the ceria-AA and ceria-CAN samples. The smaller ceria-CAN nanoparticles dissolve faster because of their higher photodissolution quantum yields (see below). For the ceria-AA sample (Figure 4a), the normalized difference spectra agree very well within experimental uncertainty throughout dissolution, as expected for spectra that are internally linear. The common difference spectrum agrees closely with the scaled difference spectrum calculated as the absorption spectrum of Ce^{3+}(aq) minus the absorption spectrum of the starting nanoceria solution. Given the sensitivity limit of our experiments noted above, we are confident that there are no size-dependent changes to the absorption spectra of fully oxidized ceria nanoparticles at least down to the level of particles with a diameter of 1.5 nm throughout the wavelength range shown in Figure 2. This reinforces the conclusion that absorption by many metal oxides involves localized charge transfer transitions.[65]

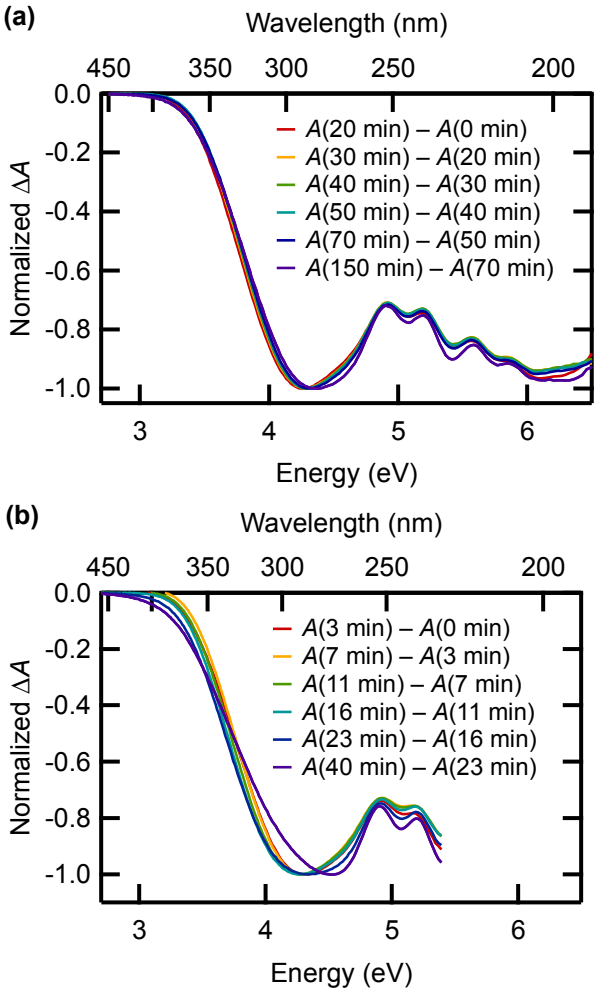

Figure 4. Normalized difference spectra taken during irradiation of (a) ceria-AA and (b) ceria-CAN, calculated from the solution absorbance measured at the times shown in the legend. The difference spectra for ceria-CAN are restricted to $\lambda > 230$ nm due to interfering absorption by nitrate ions at shorter wavelengths.

In contrast to the nearly unchanging difference spectra of the ceria-AA nanoparticles (Figure 4a), the normalized difference spectra for the ceria-CAN sample do change with irradiation time (Figure 4b), beginning with the very first difference spectrum. The normalized difference spectra show increased tailing at wavelengths longer than 350 nm as t_2 increases

(Figure 4b), indicating that the absorption spectrum of the ceria that dissolves during later time intervals is red-shifted from the absorption spectrum of ceria dissolved during earlier time intervals. In other words, the absorption spectrum of smaller ceria-CAN nanoparticles has increased absorption at wavelengths longer than 350 nm.

We do not believe that the changes in Figure 4b are due to quantum confinement because no changes are seen for the ceria-AA nanoparticles as they pass through a similar size regime. Instead, we propose that the weak red shifting in the smaller ceria-CAN nanoparticles is a result of their polycrystallinity. Prior studies have shown that absorption by amorphous ceria and amorphous Ce^{4+} oxyhydroxides is broader and weaker than that of crystalline ceria.[46, 66] We suggest that hydroxylation contributes to the long wavelength tail absorption of ceria as has been observed near the surface of iron(III) oxides.[67] The reduced crystallinity of the ceria-CAN nanoparticles prior to their photodissolution is also responsible in our view for their greater long-wavelength tail absorption and for their lower absorption coefficient near the band maximum compared to the more crystalline ceria-AA particles (Figure 1).

Photoreduction quantum yields. The quantum yield of photoreduction (moles of Ce^{3+} formed per mole of absorbed photons) was estimated from the initial change in absorbance at 290 nm with UV irradiation as described in section 1 of the SI. Quantum yield measurements were made for each ceria sample at 265 and 300 nm with and without 1 M glycerol. Glycerol efficiently scavenges photogenerated holes in TiO_2 nanoparticles.[68] The faint yellow color of the ceria-CAN nanoparticle suspension darkens slightly upon addition of glycerol, consistent with the modest red shift seen in the UV-vis spectrum (Figure S10a). In contrast, the UV-vis spectrum of the ceria-AA sample changes negligibly with the addition of 1 M glycerol (Figure S10b) as the relative fraction of Ce ions on the surface is lower in these larger particles.

Importantly, the measured quantum yield is for bleaching due to the photoreduction of Ce^{4+} to Ce^{3+}. This could differ from the quantum yield of photodissolution if Ce^{3+} ions could be deeply trapped at a grain boundary in the nanoparticle interior. As argued earlier, however, the excellent internal linearity observed during photodissolution rules out any blue shifting of the absorption maximum like that observed when Ce^{3+} ions stably accumulate near the surface in nanoceria at higher pH values (Figure 3b). If we assume that Ce^{3+} ions in nanoceria absorb the same in the interior as near the surface, then Ce^{3+} defects must be present in very low quantities at low pH given the absence of blue shifting. In this case, the measured quantum yield of photoreduction is likely to equal the quantum yield of photodissolution.

The measured quantum yields, which are summarized in Table 1, show several trends: 1) The smaller ceria-CAN nanoparticles consistently have quantum yields that are two times higher than for the ceria-AA particles under the same experimental conditions, 2) the addition of 1 M glycerol causes the quantum yield to increase by a factor of between three and six at both excitation wavelengths, and 3) for each sample, decreasing the excitation wavelength from 300 nm to 265 nm increases the photoreductive dissolution quantum yield by a factor of two to three with or without glycerol. We note that the effects of excitation wavelength and added glycerol are independent. Thus, decreasing the excitation wavelength from 300 to 265 nm and adding 1 M glycerol causes the quantum yield of photoreductive dissolution to increase by approximately one order of magnitude in both nanoceria samples.

The quantum yields in Table 1 range between 4 and 68% and are generally higher than has been reported for other metal oxides to the best of our knowledge. For example, a value of just 3% was reported for the quantum yield of photoreduction of < 3 nm diameter anatase TiO_2 nanoparticles in the presence of the hole scavenger ethanol with UV excitation from 300 to 400

nm.[25] Table 1 indicates that photoreduction is approximately one order of magnitude more efficient in nanoceria. The quantum yields reported for the photoreductive dissolution of iron oxide in the presence of an organic electron donor adsorbed on the nanoparticle surface are less than a few percent[42, 67] and are much smaller than the quantum yields observed here for nanoceria even in the absence of a good electron donor. The quantum yields of photoreduction in Table 1 reveal that a significant fraction of photogenerated electron hole pairs escape recombination in ceria nanoparticles. In contrast, 90% of photogenerated electron-hole pairs are reported to recombine in TiO_2 under UV excitation.[69]

Table 1. Photoreduction quantum yields of the nanoceria samples studied.[a]

λ / nm	**Ceria-CAN**	**Ceria-CAN, 1 M Glycerol**	**Ceria-AA**	**Ceria-AA, 1 M Glycerol**
265	0.18	0.68	0.08	0.37
300	0.060	0.33	0.042	0.15

[a]Measured in pH 1.9 ± 0.1 aqueous suspensions at the wavelengths indicated. The relative uncertainty in the quantum yields is estimated to be 10% from ≥ 3 independent trials.

These initial results show that the quantum yields depend strongly on nanoparticle size, excitation wavelength, and on the presence of a hole scavenger (glycerol) on the nanoparticle surface. We offer next some initial explanations for these trends, although establishing detailed mechanisms is a task for future studies. First, the quantum yield of photoreduction is roughly twice as large for ceria-CAN vs. ceria-AA with or without added glycerol (Table 1), and this

agrees with the larger surface area-to-volume ratio of the ceria-CAN particles. The probability of forming an excitation at the surface should be greater for smaller nanoparticles given that the absorption cross section per formula unit of CeO_2 appears to be independent of nanoparticle size. Additionally, the initial quantum yields could be affected by the roughness of the particle surface.

Photoreduction of colloidal anatase TiO_2 cannot be observed in aqueous solution without a hole scavenger.[25] Prompt hole scavenging is likely to be a requirement for lasting photoreduction or photodissolution as removal of the hole from the particle prevents recombination. The different passivating ligands on the ceria-CAN and ceria-AA nanoparticles could act as terminal hole scavengers or electron donors. Thermodynamic considerations suggest that water molecules or bound hydroxide ions could also play this role, and further studies are needed to decide among these possibilities. The hole in nanoceria can be transferred to a water molecule in the solvent by either of the following reactions, which describe the net dissolution of one formula unit from a photoexcited ceria nanoparticle, CeO_2^*,

$$CeO_2^* + H_2O + 3\ H^+ \rightarrow\ Ce^{3+}(aq) + \cdot OH + 2H_2O \qquad (2)$$

$$CeO_2^* + H_2O + 3H^+ \rightarrow\ Ce^{3+}(aq) + ¼\ O_2 + 5/2\ H_2O\ . \qquad (3)$$

An analogous reaction can be written in which a hydroxide ion bound to the nanoparticle is oxidized. In reaction 2, water undergoes one electron oxidation to the hydroxyl radical, while in reaction 3, water undergoes four-electron oxidation to O_2. According to either of the above reactions, three moles of protons are consumed for every mole of Ce^{3+}, released to the solution. A rise in pH, was observed in our initial experiments, but because this triggered nanoparticle aggregation that interfered with the measurements, perchloric acid was added in all later experiments to maintain nearly constant pH throughout dissolution.

In CeO_2, unlike in TiO_2, nearly every hole formed near the surface may be capable of oxidizing a water or hydroxide ion. As summarized in Table 1 of ref. 70, trapping reduces the oxidizing potential of the initial valence band hole in TiO_2 from approximately +2.96 V vs. NHE at pH 2 to approximately 1.6 V for the trapped hole, an effect that has been reproduced by theory.[71] We speculate that surface-localized holes in nanoceria have greater oxidizing power than ones in TiO_2, allowing rapid one-electron oxidation of a bound water molecule or hydroxide ion. Further work is needed to address this issue.

The higher quantum yields seen for smaller particles and the ability of a surface adsorbate (glycerol) to increase quantum yields confirm that the proximity of the initial excitation to the surface is correlated with long-lived charge separation. The lower yields observed without a scavenger suggest that electron-hole recombination does compete with dissolution. The increased yields seen at 300 vs. 265 nm suggest further that shorter excitation wavelengths also inhibit electron-hole recombination. As excitations are expected to thermalize with the lattice in no more than a few ps, this indicates that events taking place on shorter time scales are the key to generating separated carriers. Thus, excess energy may help a hole to reach the surface before it loses too much free energy and is unable to oxidize a bound water molecule or hydroxide ion.

CONCLUSIONS

Although photoreductive dissolution will limit applications of photoexcited nanoceria in highly acidic conditions, this phenomenon and its high quantum efficiency were used to obtain important insights into the behavior of photogenerated electron-hole pairs of importance for photocatalysis and to reconcile controversies about the absorption characteristics of nanoceria. Using only light to change the size of ceria nanoparticles that are fully oxidized, we showed that

quantum confinement effects are not observed for small clusters containing no more than several tens of Ce ions.

We have shown that UV irradiation of ceria nanoparticles efficiently forms very long-lived Ce^{3+} centers. These are released into the solution if the pH is less than ~3, causing the particles to reductively dissolve and shrink, but are retained in the nanoparticles if the solution is less acidic. For particles of any size, nearly every metal ion at the surface can be reduced. This implies that a greater fraction of cerium ions can be reduced in smaller particles. The quantum yields of photoreduction, which we suggest roughly equal those of photodissolution at low pH, are the highest reported for metal oxide nanoparticles to the best of our knowledge. Furthermore, photoreduction does not require an added electron donor because holes in ceria appear to readily oxidize water molecules or hydroxide ions adsorbed to the nanoparticle surface.

While small ceria nanoparticles have a great potential for hosting a high fraction of Ce^{3+} defects, whether they actually do or not depends strongly on extrinsic factors such as X-ray or UV exposure and on the presence of oxygen vacancies. Our results show that the fully oxidized state of nanoparticles < 10 nm in diameter can be maintained even as particles are shrunk down to molecular-sized clusters. The possibility that the Ce^{3+} content of nanoceria is not fixed by particle size, but can be manipulated over a considerable range should be taken into account when nanoceria is used for catalysis.

The phenomenon of photoreductive dissolution is also important for understanding the dynamics of photogenerated carriers in ceria because every Ce^{3+} ion that desorbs or remains stably trapped is the product of an electron-hole pair that did not recombine. The insight that small ceria nanoparticles can be prepared essentially free of Ce^{3+} defects in acidic aqueous

solution should benefit future efforts that aim to characterize carrier dynamics in nanoceria using time-resolved laser spectroscopy.

ACKNOWLEDGEMENTS

Acknowledgment is made to the donors of the American Chemical Society Petroleum Research Fund for support of this research. NP gratefully acknowledges support as an NSF Graduate Research Fellow under Grant No. 1049562. SF is grateful for a Feodor Lynen Research Fellowship by the Alexander von Humboldt Foundation. We thank Robert E. A. Williams of Ohio State University's Center for Electron Microscopy and Analysis for his assistance with HR-TEM measurements. We also thank Ohio State undergraduate Brian Wynne for help with the initial quantum yield measurements.

REFERENCES

1. A. Ruiz Puigdollers, P. Schlexer, S. Tosoni and G. Pacchioni, *ACS Catal.*, 2017, **7**, 6493-6513.

2. T. Montini, M. Melchionna, M. Monai and P. Fornasiero, *Chem. Rev.*, 2016, **116**, 5987-6041.

3. M. V. Ganduglia-Pirovano, A. Hofmann and J. Sauer, *Surf. Sci. Rep.*, 2007, **62**, 219-270.

4. S. Yabe and T. Sato, *J. Solid State Chem.*, 2003, **171**, 7-11.

5. J. M. Coronado, A. Javier Maira, A. Martínez-Arias, J. C. Conesa and J. Soria, *J. Photochem. Photobiol. A: Chem.*, 2002, **150**, 213-221.

6. N. M. Zholobak, V. K. Ivanov, A. B. Shcherbakov, A. S. Shaporev, O. S. Polezhaeva, A. Y. Baranchikov, N. Y. Spivak and Y. D. Tretyakov, *J. Photochem. Photobiology B-Biology*, 2011, **102**, 32-38.

7. Y. Z. Li, Q. Sun, M. Kong, W. Q. Shi, J. C. Huang, J. W. Tang and X. J. Zhao, *J. Phys. Chem. C*, 2011, **115**, 14050-14057.

8. C. Yang, X. Yu, P. N. Pleßow, S. Heißler, P. G. Weidler, A. Nefedov, F. Studt, Y. Wang and C. Wöll, *Angew. Chem. Int. Ed.*, 2017, **56**, 14301-14305.

9. D. Channei, S. Phanichphant, A. Nakaruk, S. S. Mofarah, P. Koshy and C. C. Sorrell, *Catalysts*, 2017, **7**, 23.

10. S. L. Xie, Z. L. Wang, F. L. Cheng, P. Zhang, W. J. Mai and Y. X. Tong, *Nano Energy*, 2017, **34**, 313-337.

11. C. Korsvik, S. Patil, S. Seal and W. T. Self, *Chem. Commun.*, 2007, 1056-1058.

12. T. Xia, M. Kovochich, M. Liong, L. Maedler, B. Gilbert, H. Shi, J. I. Yeh, J. I. Zink and A. E. Nel, *ACS Nano*, 2008, **2**, 2121-2134.

13. T. Pirmohamed, J. M. Dowding, S. Singh, B. Wasserman, E. Heckert, A. S. Karakoti, J. E. S. King, S. Seal and W. T. Self, *Chem. Commun.*, 2010, **46**, 2736-2738.

14. I. Celardo, J. Z. Pedersen, E. Traversa and L. Ghibelli, *Nanoscale*, 2011, **3**, 1411-1420.

15. S. S. Lee, W. Song, M. Cho, H. L. Puppala, P. Nguyen, H. Zhu, L. Segatori and V. L. Colvin, *ACS Nano*, 2013, **7**, 9693-9703.

16. P. Ni, X. S. Wei, J. Guo, X. R. Ye and S. Yang, *RSC Adv.*, 2015, **5**, 97512-97519.

17. A. Dhall and W. Self, *Antioxidants*, 2018, **7**, 13.

18. I. Celardo, M. De Nicola, C. Mandoli, J. Z. Pedersen, E. Traversa and L. Ghibelli, *ACS Nano*, 2011, **5**, 4537-4549.

19. S. Tsunekawa, T. Fukuda and A. Kasuya, *Surf. Sci.*, 2000, **457**, L437-L440.

20. L. Wu, H. J. Wiesmann, A. R. Moodenbaugh, R. F. Klie, Y. Zhu, D. O. Welch and M. Suenaga, *Phys. Rev. B*, 2004, **69**, 125415.

21. S. Deshpande, S. Patil, S. Kuchibhatla and S. Seal, *Appl. Phys. Lett.*, 2005, **87**, 3.

22. S. S. Lee, H. G. Zhu, E. Q. Contreras, A. Prakash, H. L. Puppala and V. L. Colvin, *Chem. Mater.*, 2012, **24**, 424-432.

23. C. Paun, O. V. Safonova, J. Szlachetko, P. M. Abdala, M. Nachtegaal, J. Sa, E. Kleymenov, A. Cervellino, F. Krumeich and J. A. van Bokhoven, *J. Phys. Chem. C*, 2012, **116**, 7312-7317.

24. F. Zhang, P. Wang, J. Koberstein, S. Khalid and S. W. Chan, *Surf. Sci.*, 2004, **563**, 74-82.

25. C. Kormann, D. W. Bahnemann and M. R. Hoffmann, *J. Phys. Chem.*, 1988, **92**, 5196-5201.

26. C. A. Leatherdale, W. K. Woo, F. V. Mikulec and M. G. Bawendi, *J. Phys. Chem. B*, 2002, **106**, 7619-7622.

27. C. Xia, W. Wu, T. Yu, X. Xie, C. van Oversteeg, H. C. Gerritsen and C. de Mello Donega, *ACS Nano*, 2018, **12**, 8350-8361.

28. L. X. Yin, Y. Q. Wang, G. S. Pang, Y. Koltypin and A. Gedanken, *J. Colloid Interface Sci.*, 2002, **246**, 78-84.

29. N. S. Arul, D. Mangalaraj, P. C. Chen, N. Ponpandian and C. Viswanathan, *Mater. Lett.*, 2011, **65**, 2635-2638.

30. R. Qing and W. Sigmund, *Journal of Photochemistry and Photobiology A: Chemistry*, 2013, **266**, 55-63.

31. T. Masui, K. Fujiwara, K. Machida, G. Adachi, T. Sakata and H. Mori, *Chem. Mater.*, 1997, **9**, 2197-2204.

32. T. Suzuki, I. Kosacki, V. Petrovsky and H. U. Anderson, *J. Appl. Phys.*, 2002, **91**, 2308-2314.

33. P. Patsalas, S. Logothetidis, L. Sygellou and S. Kennou, *Phys. Rev. B*, 2003, **68**, 035104.

34. M. D. Hernandez-Alonso, A. B. Hungria, A. Martinez-Arias, J. M. Coronado, J. C. Conesa, J. Soria and M. Fernandez-Garcia, *Phys. Chem. Chem. Phys.*, 2004, **6**, 3524-3529.

35. S. Tsunekawa, T. Fukuda and A. Kasuya, *J. Appl. Phys.*, 2000, **87**, 1318-1321.

36. S. Tsunekawa, J. T. Wang, Y. Kawazoe and A. Kasuya, *J. Appl. Phys.*, 2003, **94**, 3654-3656.

37. D. Damatov, S. M. Laga, E. A. Mader, J. Peng, R. G. Agarwal and J. M. Mayer, *Inorg. Chem.*, 2018, **57**, 14401-14408.

38. V. K. Klochkov, Y. V. Malyukin, G. V. Grygorova, O. O. Sedyh, N. S. Kavok, V. V. Seminko and V. P. Semynozhenko, *J. Photochem. Photobiol. A-Chem.*, 2018, **364**, 282-287.

39. U. Schwertmann, *Plant Soil*, 1991, **130**, 1-25.

40. D. Suter, S. Banwart and W. Stumm, *Langmuir*, 1991, **7**, 809-813.

41. W. Stumm and B. Sulzberger, *Geochim. Cosmochim. Acta*, 1992, **56**, 3233-3257.

42. C. Siffert and B. Sulzberger, *Langmuir*, 1991, **7**, 1627-1634.

43. H. Fu, D. M. Cwiertny, G. R. Carmichael, M. M. Scherer and V. H. Grassian, *Journal of Geophysical Research: Atmospheres*, 2010, **115**.

44. J. A. Soltis, A. M. Schwartzberg, P. Zarzycki, R. L. Penn, K. M. Rosso and B. Gilbert, *ACS Earth and Space Chemistry*, 2017, **1**, 216-226.

45. A. G. Xyla, B. Sulzberger, G. W. Luther, J. G. Hering, P. Vancappellen and W. Stumm, *Langmuir*, 1992, **8**, 95-103.

46. N. W. Pettinger, R. E. A. Williams, J. Chen and B. Kohler, *Phys. Chem. Chem. Phys.*, 2017, **19**, 3523-3531.

47. C. K. Jørgensen and J. S. Brinen, *Mol. Phys.*, 1963, **6**, 629-631.

48. Y. Kaizu, K. Miyakawa, K. Okada, H. Kobayashi, M. Sumitani and K. Yoshihara, *J. Am. Chem. Soc.*, 1985, **107**, 2622-2626.

49. J. Brynestad and G. P. Smith, *J. Phys. Chem.*, 1968, **72**, 296-300.

50. L. J. Heidt and M. E. Smith, *J. Am. Chem. Soc.*, 1948, **70**, 2476-2481.

51. P. Lommens, K. Lambert, F. Loncke, D. De Muynck, T. Balkan, F. Vanhaecke, H. Vrielinck, F. Callens and Z. Hens, *ChemPhysChem*, 2008, **9**, 484-491.

52. A. Sehgal, Y. Lalatonne, J. F. Berret and M. Morvan, *Langmuir*, 2005, **21**, 9359-9364.

53. A. M. Schimpf, C. E. Gunthardt, J. D. Rinehart, J. M. Mayer and D. R. Gamelin, *J. Am. Chem. Soc.*, 2013, **135**, 16569-16577.

54. P. Yu, S. A. Hayes, T. J. O'Keefe, M. J. O'Keefe and J. O. Stoffer, *J. Electrochem. Soc.*, 2006, **153**, C74-C79.

55. H. I. Chen and H. Y. Chang, *Colloids and Surfaces a-Physicochemical and Engineering Aspects*, 2004, **242**, 61-69.

56. T. V. Plakhova, A. Y. Romanchuk, S. N. Yakunin, T. Dumas, S. Demir, S. A. Wang, S. G. Minasian, D. K. Shuh, T. Tyliszczak, A. A. Shiryaev, A. V. Egorov, V. K. Ivanov and S. N. Kalmykov, *J. Phys. Chem. C*, 2016, **120**, 22615-22626.

57. Y. Peng, X. Chen, G. Yi and Z. Gao, *Chem. Commun.*, 2011, **47**, 2916-2918.

58. F. Schwabe, R. Schulin, P. Rupper, A. Rotzetter, W. Stark and B. Nowack, *J. Nanopart. Res.*, 2014, **16**, 2668.

59. L. Sun, X. Huang, L. Wang and A. Janotti, *Phys. Rev. B*, 2017, **95**, 245101.

60. H. L. Tuller and A. S. Nowick, *J. Phys. Chem. Solids*, 1977, **38**, 859-867.

61. J. J. Plata, A. M. Marquez and J. F. Sanz, *J. Phys. Chem. C*, 2013, **117**, 14502-14509.

62. C. W. M. Castleton, A. Lee and J. Kullgren, *J. Phys. Chem. C*, 2019, **123**, 5164-5175.

63. B. Goris, S. Turner, S. Bals and G. Van Tendeloo, *ACS Nano*, 2014, **8**, 10878-10884.

64. T. Ghoshal, P. G. Fleming, J. D. Holmes and M. A. Morris, *J. Mater. Chem.*, 2012, **22**, 22949-22957.

65. S. Biswas, J. Husek, S. Londo and L. R. Baker, *Nano Lett.*, 2018, **18**, 1228-1233.

66. S. Guo, H. Arwin, S. N. Jacobsen, K. Järrendahl and U. Helmersson, *J. Appl. Phys.*, 1995, **77**, 5369-5376.

67. B. C. Faust and M. R. Hoffmann, *Environmental Science & Technology*, 1986, **20**, 943-948.

68. I. A. Shkrob and M. C. Sauer, *J. Phys. Chem. B*, 2004, **108**, 12497-12511.

69. J. Schneider, M. Matsuoka, M. Takeuchi, J. L. Zhang, Y. Horiuchi, M. Anpo and D. W. Bahnemann, *Chem. Rev.*, 2014, **114**, 9919-9986.

70. T. Tachikawa, M. Fujitsuka and T. Majima, *J. Phys. Chem. C*, 2007, **111**, 5259-5275.

71. C. Di Valentin and A. Selloni, *J. Phys. Chem. Lett.*, 2011, **2**, 2223-2228.